Yield Characteristics of a Twill Dutch Woven Wire Mesh Via Experiments and Numerical Modeling

Steven M. Kraft

Ali P. Gordon

Department of Mechanical, Materials, and Aerospace Engineering, University of Central Florida, Orlando, FL 32816-2450

Woven structures are steadily emerging as excellent reinforcing components in composite materials. Metallic woven meshes, unlike most woven fabrics, show high potential for strengthening via classical methods such as heat treatment. Development of strengthening processes for metallic woven materials, however, must account not only for behavior of the constituent wires, but also for the interactions between contacting wires. Yield behavior of a 325 × 2300 stainless steel 316L (SS316L) twill dutch woven wire mesh is analyzed via experimental data and 3D numerical modeling. The effects of short dwell-time heat treatment on the mechanical properties of this class of materials is investigated via uniaxial tensile tests in the main weave orientations. Scanning electron microscopy (SEM) is employed to investigate the effects of heat treatment on contacting wire interaction, prompted by observations of reduced ductility in the macrostructure of the mesh. Finally, the finite element method (FEM) is used to simulate the accumulation of plastic deformation in the mesostructure of the mesh, investigating how this wire level plasticity ultimately affects global material yielding. [DOI: 10.1115/1.4007793]

1 Introduction

As composite materials continue to move into the forefront in both industrial and aerospace applications, woven fiber geometries are emerging as ideal reinforcing materials. While woven materials show great potential in composites and other applications, a complete understanding of their governing mechanics is still evolving. Several researchers have contributed to the study of fabric behavior, most notably in the form of tensile testing [1–4] and finite element modeling [5–8]. The work presented here expands on research previously published by the authors [9], which focused on defining the mechanical properties of a 325×2300 SS316L twill dutch woven wire mesh through uniaxial tensile experiments and main axes (warp and weft) finite element modeling. Extensions have been made to this ongoing research to characterize the effect of short dwell time heat treatment on the mechanical properties of the mesh, and to extend modeling efforts to off-axis cases. A short dwell-time heat treatment was chosen in an effort to reproduce Explosive Trace Detection (ETD) type service conditions of this material. Experimental results from heat treated main axes specimens are analyzed to investigate observed changes in ductility and strength. Also, numerical simulations are broadened to incorporate all experimentally tested material orientations. These numerical results are used to investigate the yielding behavior of the woven mesh with respect to the accumulation of plastic deformation at the wire level.

The most common mechanical testing approach for fabrics in the literature is the uniaxial tensile test. Typically, these tests are performed in the main weave directions and at several intermediate orientations. This technique enables the researcher to fully define the orthotropic properties of the material with a simple and inexpensive mechanical test. Alternatively, biaxial mechanical testing can be performed on cruciform specimens [2,5]. This method of testing is ideal in that the results are not adversely affected by shear coupling [10]; however, difficulties arise in the form of cruciform specimen limitations [11], and the need for more sophisticated testing devices [5,12].

As is often the case with composite materials, fabrics pose a challenge in the definition of mechanical properties due to their inhomogeneous structure. The relationship between mechanical behavior of the mesostructure, typically treated as one weave period, and the macroscale response are often times unclear, and little information linking the two scales can be gained from simple mechanical testing. To address this issue, the finite element method (FEM) has been used extensively in literature to model the mesoscale behavior of fabric materials. Tarfoui and coworkers [6] employed finite elements to study an idealized fabric structure at the mesoscale, and ultimately utilized the model to make damage predictions. Other notable research efforts using finite elements to study mesoscale fabric behavior have been made by Cavellero and coworkers [5], Nicoletto and coworkers [7], and Barbero and co-authors [8]. The relatively large body of research in this area has proven FEM to be a reasonable approach to modeling complex fabric behavior, with a major limit being model size and inevitable boundary influence on model response. The model developed in this research is much larger than the typical representative volume element models in the literature, with the goal of alleviating some boundary condition influence on response.

This paper presents results from detailed 3D numerical modeling of a 325×2300 twill dutch woven wire mesh, and an extension of mechanical testing results from a prior study to include heat treated specimens. The effect of short dwell-time heat treatment on the mechanical response of the woven wire mesh is investigated via uniaxial tensile testing in the main material orientations, and observations are made regarding the effectiveness of such treatments to enhance material properties, particularly yield strength. Evolution of local plastic strain in the mesostructure is simulated for several material orientations, and mesoscale wire yielding is compared to macroscale mesh yield behavior obtained from uniaxial tensile experiments.

2 The Woven Wire Mesh

The material of interest in this study is a micronic twill dutch woven wire mesh. This material is frequently used in fine filtration applications where it is exposed to biaxial loads in the form of hydrodynamic pressure, as well as temperature gradients and

Manuscript received April 1, 2011; final manuscript received April 18, 2012; accepted manuscript posted October 10, 2012; published online May 16, 2013. Assoc. Editor: Vikram Deshpande.

Table 1 Material properties of bulk stainless steel 316 L at room temperature [13]

Units	Elastic modulus, E	Yield strength, σ_y	Ultimate tensile strength, UTS	Density, ρ	Elongation, ε_f (%)	Poisson's ratio, ν
SI	193 GPa	205 MPa	520 MPa	0.008 g/mm^3	40	0.28
English	28.0 Msi	29.7 ksi	75.4 ksi	0.289 lbf/in^3	40	0.28

particle deposition. Recently, this material has been employed in Explosive Trace Detection (ETD) applications in which it is simultaneously exposed to extreme temperature gradients and hydrodynamic forces. The mesh is woven from SS316L wires, giving it superb tolerance to thermal shock and repeated loading cycles. The material properties of AISI for bulk SS316L are provided in Table 1 [13]. It is noted, however, that material strength in wires tends to increase with decreasing diameter, i.e.,

$$S_{ut} = Ad^{-m} \tag{1}$$

where A and m are material properties, and d is the wire diameter. The wires making up the woven mesh in question are of the order of one thousandth of an inch (25.4 μm) in diameter, resulting in wire strengths much higher than listed in Table 1.

The SS316L wires are woven into the mesh in a twill dutch fashion, where the term twill reflects that the weft (shute) wires are woven in a two under, two over pattern with respect to the warp (toe) wires, and the term dutch communicates that the weft wires are of a smaller diameter than the warp wires. This weave pattern produces an extremely tight mesh, with nominal and absolute pore sizes of 2 and 7 μm, respectively. While this weaving pattern enhances the effectiveness of the mesh as a filtration media, the torturous weaving process also causes significant damage to the wires, as evidenced by the areas of plastic deformation highlighted in the scanning electron microscopy (SEM) image shown in Fig. 1. This wire damage undoubtedly causes a reduction in global strength of the mesh, and there is significant potential that this problem could be alleviated by heat treatment of the mesh to reduce residual stresses caused by the weaving process. Figure 1 also illustrates the woven wire mesh and defines all key dimensions, summarized in detail in Table 2. The ASTM standard E2016 (2006) provides the equations used to arrive at the reported weight values for the mesh.

3 Tensile Testing

Uniaxial tensile experiments were conducted on strip specimens of the 325 × 2300 SS316L woven wire mesh in the main wire orientations, hereby referred to as the warp (0 deg) and the

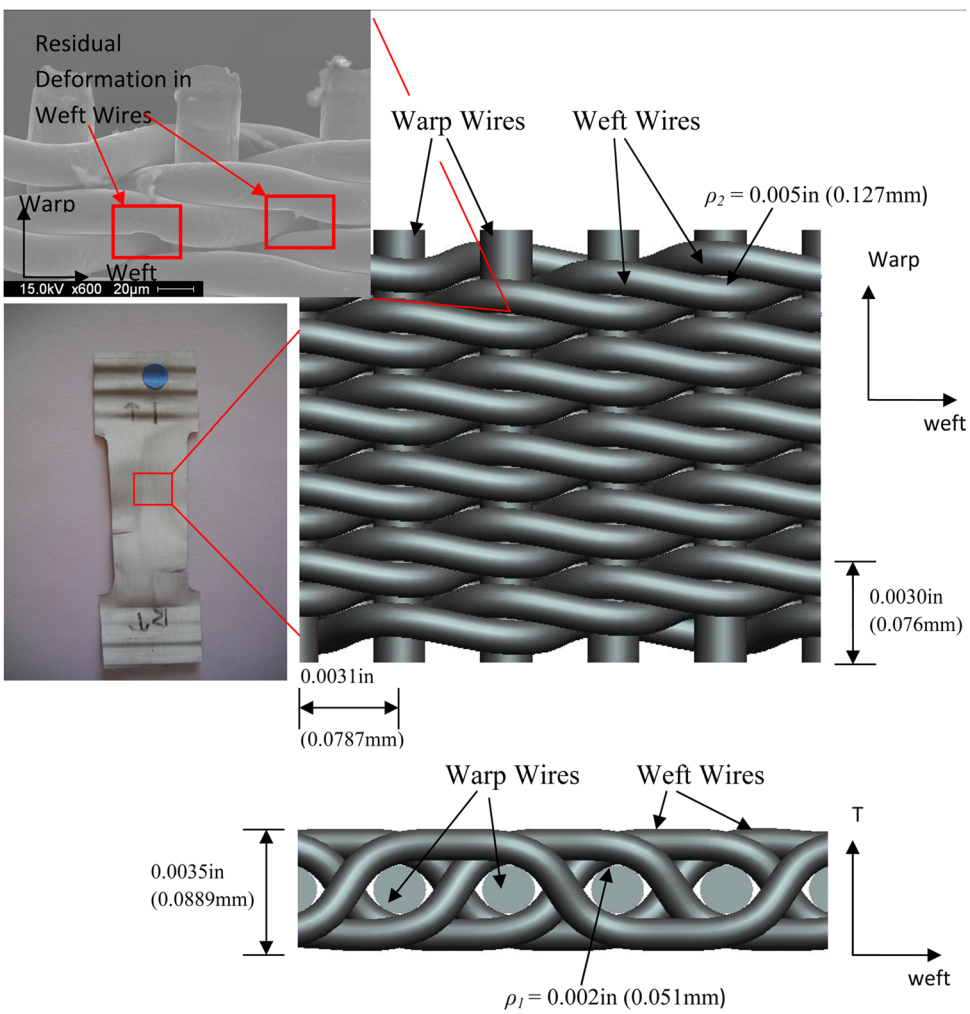

Fig. 1 Images and rendering of the 325 × 2300 SS316L twill dutch woven wire mesh specimen and weave geometry outlining key dimensions

Table 2 325 × 2300 316L SS woven wire mesh specifications

Units	Warp wire count, N_s	Weft wire count, N_w	Warp wire diameter, D_s	Weft wire diameter, D_w	Mesh thickness, T	Mesh weight, W
English	325 wires/in.	2300 wires/in.	0.0015 in.	0.0010 in.	0.0035 in.	0.099 lb/ft^2
SI	127 wires/cm	905 wires/cm	0.0381 mm	0.0254 mm	0.0889 mm	483.4 g/m^2

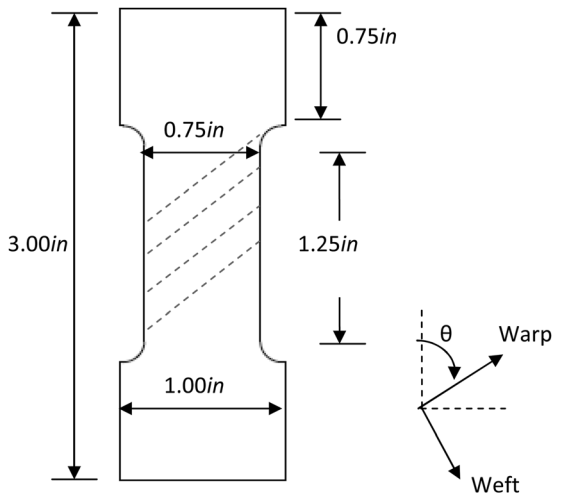

Fig. 2 Dog-bone test specimens used in uniaxial tensile experiments conducted on the 325 × 2300 SS316L twill dutch woven wire mesh

weft (90 deg) directions, and at several orientations in between. These tests were carried out using an MTS Insight 5 electromechanical uniaxial testing machine, using a constant rate of extension (CRE) test method at 0.10 in/min (2.54 mm/min), as specified by ASTM Standard D4964 (2008). The device allowed for the acquisition of the load versus displacement response of each specimen, which could then be used to ascertain numerous material properties such as stiffness, yield strength, ultimate strength, toughness, elongation to failure, etc.

3.1 Test Specimens. The woven wire mesh specimens were incised from larger material sheets by hand into the standard dog-bone shape as per ASTM Standard E8 (2004). The specimens were iteratively designed to ensure optimal failure in the gauge section of the specimen, and this was the case in the majority of the test runs. The optimal test specimen geometry is provided as Fig. 2, with a gauge width of 0.75 in. (19.05 mm.) and a gauge length of 1.25 in. (31.75 mm.). This specimen geometry produces an active (load bearing) wire count of 243 warp wires in the warp (0 deg) orientation, and 1725 weft wires in the weft (90 deg) orientation. Specimens were held by wave-shaped grips (Test Resources Model No.G86G) suitable for gripping the very thin material samples.

Incision of the test samples by hand inherently introduces variability into the specimen geometry that could ultimately influence test results. To gauge the level of variability in these experiments arising from, among other possible factors, sample geometry, a series of ten tensile tests were initially run to fracture on warp (0 deg) specimens. The results of this specimen variability testing are provided in Table 3 [9], where the values have been normalized such that $A_0 = 0.00248$ in^2 (1.60 mm^2), $k_0 = 2327$ lb/in (407.5 kN/m), $S_{y0} = 11.4$ ksi (78.6 MPa), $UTS_0 = 12.7$ ksi (87.6 MPa), $S_{f0} = 11.9$ ksi (82.0 MPa), and $\varepsilon_{fo} = 0.084$ in (2.13 mm). Note that the cross-sectional area, A_0, represents the cross section of the material as if it were a homogenous body. The highest degree of standard deviation observed in the normalized data was in the elongation to failure, with an acceptable value of 0.12. Yield strength and stiffness also show notable normalized standard deviations, with values of 0.04 and 0.10, respectively. These values are considered within statistical error limits for mechanical testing of this class of materials, and so it was justified to proceed with further testing of the material without multiple test duplications.

Specimens were incised in both the warp (0 deg) and weft (90 deg) material orientations, and at off-axis angles in 15 deg intervals, as illustrated by Fig. 2. This approach produces detailed information on the orientation dependence of material properties such as yield strength and elastic modulus, and allows for the application of classical mechanical models to the material through regression analysis or other means [4,9].

As the specimen orientation diverges from the main weave axes, edge effects due to wire cut-off are unavoidable. This problem is most pronounced in the 45 deg orientation, where a typical aspect-ratio dogbone shaped specimen could potentially have no wires that run the entire gauge length. The authors have given much attention to the effects of widening the sample specimen to reduce edge effects in a previous work [9], with particular focus on how the elastic modulus and yield strength vary with orientation. From this work, it has been shown that widening the sample by a factor of two does not greatly improve material response. In fact, adverse boundary conditions that arise in clamped off-axis specimens due to shear coupling [10] are exasperated by reducing the aspect ratio of the specimens, causing failures near the specimen grips, and specimen twisting during the experiments. Future study is planned to investigate the critical length scale, i.e., the sample width at which results begin to deteriorate, for this material.

Table 3 Normalized mechanical properties of 316L SS woven wire mesh in warp (0 deg) direction

Specimen ID	Cross-sectional area, A/A_0	Stiffness, k/k_o	Yield strength, S_y/S_yo	Ultimate strength, UTS/UTS_o	Fracture stress, S_f/S_fo	Elongation, $\epsilon_f/\epsilon_{f_o}$
AR-001	1.00	1.00	0.95	1.00	1.00	1.00
AR-002	1.01	0.96	0.89	0.97	1.00	0.92
AR-003	1.01	1.08	0.98	0.98	1.00	1.04
AR-004	0.99	1.17	1.00	1.03	1.00	1.13
AR-005	0.99	1.25	0.96	1.01	1.01	0.83
AR-006	0.99	1.05	0.96	1.03	0.98	1.13
AR-007	0.99	1.24	0.97	1.01	0.98	1.04
AR-008	1.00	0.99	1.01	1.01	0.99	1.11
AR-009	0.99	1.17	0.98	1.04	1.00	1.08
AR-010	1.00	1.05	1.02	1.03	0.98	1.25

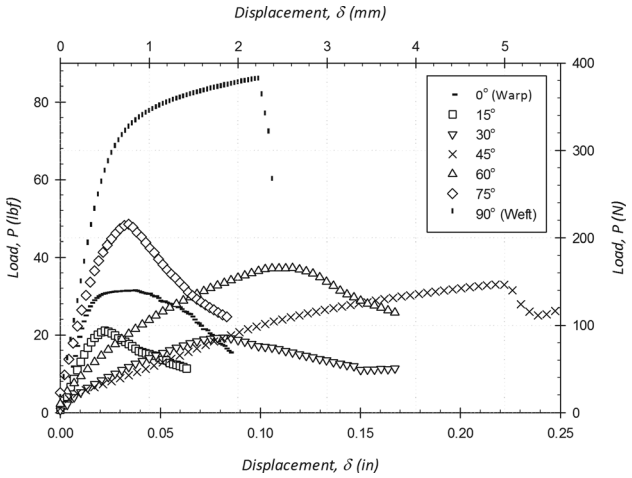

Fig. 3 Mechanical response of the 325 × 2300 SS316L twill dutch woven wire mesh at various material orientations, with 0 deg indicating the warp direction, and 90 deg indicating the weft direction

3.2 As Woven Specimen Results. The material response of the 325 × 2300 SS316L woven wire mesh in various material orientations is provided in Fig. 3. Several material properties for the as-received woven wire mesh have been established from the experimental data, and these properties are defined in Table 4 [9]. Note that properties presented here are normalized as in Table 3. Thorough review and analysis of the as-received woven wire mesh tensile test results has been conducted by the authors in previous work [9], and it is presented here in summarized form for the sake of continuity and completeness. It is noted that maximum stiffness, yield strength, and ultimate strength are observed in the weft (90 deg) direction at 2.88 kip/in (504.0 kN/m), 23.0 ksi (158.6 MPa) and 34.4 ksi (237.2 MPa), respectively. The warp (0 deg) orientation shows the least elongation to fracture, and very little potential for work hardening.

3.3 The Applied Heat Treatment. Metallic woven materials in general are excellent candidates for strengthening via heat treatment. This class of material is often exposed to cyclic, short duration, high temperatures while in service, and it reasonable to assume that such exposure could have a positive impact on material properties. To investigate the application of short dwell-time heat treatment on micronic woven wire mesh materials, test specimens identical to those described in Fig. 2 were incised in both the warp (0 deg) and weft (90 deg) orientations. The specimens were then heated in a 1112.0 °F (600.0 °C) furnace for either 100 s or 200 s, typical of the high temperature exposure time seen by this material in ETD applications. Upon heating, the specimens were removed from the furnace and allowed to cool in room temperature air. The goal of this testing was to determine the impact of this short exposure time on the yield strength and stiffness of the woven wire mesh, and to investigate the feasibility of heat treatment to improve the mechanical properties of this class of material.

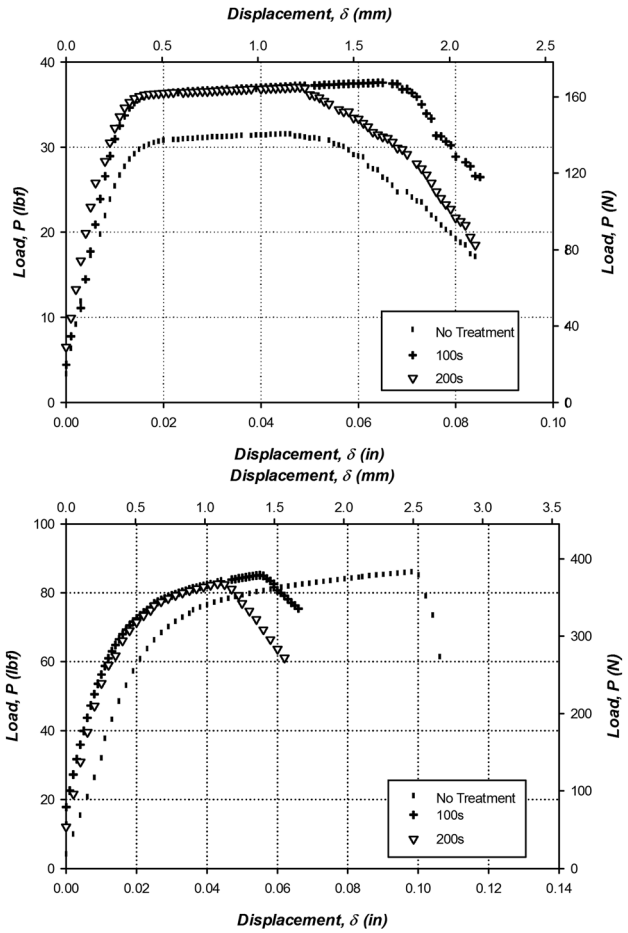

Fig. 4 The mechanical response of the main axes of the 325 × 2300 SS316L twill dutch woven wire mesh after heat treatment at 1112.0 °F (600 °C) for either 100 s or 200 s, where (*a*) is the warp (0 deg) orientation, and (*b*) is the weft (90 deg) orientation

3.4 The Effects of Heat Treatment. Careful examination of the SEM image provided in Fig. 1 reveal a significant amount of plastic deformation imparted on the wires during the weaving process. Tight weave draw down reduces weft wire cross-section at areas of adjacent wire contact by as much as 16.5%. This deformation results in residual stresses in the wires that may alter the global stiffness and yield strength of the woven wire mesh. Heat treatment is commonly employed in steel processing to relieve residual stresses and improve strength, making it a good candidate process for enhancing the material properties of the as-woven 325 × 2300 SS316L mesh.

Table 4 Orientation dependence of normalized material properties of 316L SS woven wire mesh

Specimen ID	Orientation, θ (deg)	Cross-sectional area, A/A_o	Stiffness, k/k_o	Yield strength, $\sigma_y/\sigma_y o$	Ultimate strength, UTS/UTS_o	Fracture stress, $S_f/S_f o$	Elongation, $\epsilon_f/\epsilon_{f_o}$
AR-003	0	1.01	1.08	0.98	0.98	1.00	1.04
AR-011	15	1.00	0.56	0.66	0.67	0.68	0.98
AR-012	30	1.02	0.12	0.60	0.60	0.60	3.78
AR-013	45	1.02	0.24	0.16	1.07	0.92	4.55
AR-014	60	1.02	0.20	0.96	1.16	1.21	3.30
AR-015	75	1.01	0.82	1.39	1.52	1.27	1.26
AR-016	90	1.00	1.24	2.02	2.71	2.48	1.62

Table 5 Normalized material properties for heat treated SS316L woven wire mesh samples

Specimen ID	Orientation, θ (deg)	Heating time, s	Stiffness, k/k_o	Yield strength, $\sigma_y/\sigma_y o$	Ultimate strength, UTS/UTS_o	Fracture stress, $S_f/S_f o$	Elongation, $\epsilon_f/\epsilon_{f_o}$
AR-003	0	0	1.08	0.98	0.98	1.00	1.04
AR-016	90	0	1.24	2.02	2.71	2.48	1.62
AR-017	0	100	1.27	1.16	1.18	1.19	1.15
AR-018	90	100	1.98	2.40	2.66	2.67	1.12
AR-019	0	200	1.31	1.15	1.26	1.13	1.0
AR-020	90	200	1.99	2.50	2.60	2.61	0.94

Upon a single thermal cycle of the test specimens, referred to as AR-017 through AR-020, as described, CRE tensile tests were performed at a rate of 0.1 in/min (2.54 mm/min). The mechanical response in the warp (0 deg) and weft (90 deg) orientations of the heat-treated specimens compared to the untreated specimens is shown in Figs. 4(*a*) and 4(*b*), respectively. In a similar manner as to the untreated specimens, the load versus displacement response of the treated specimens was used in conjunction with the homogenous cross-sectional area to arrive at material properties such as yield strength and ultimate strength, normalized in Table 5.

From Fig. 4, it is apparent that the applied heat treatment improves the yield strength of the woven mesh specimens in the main material axes; however, toughness and elongation to rupture are reduced as a result. The short dwell time heat treatment

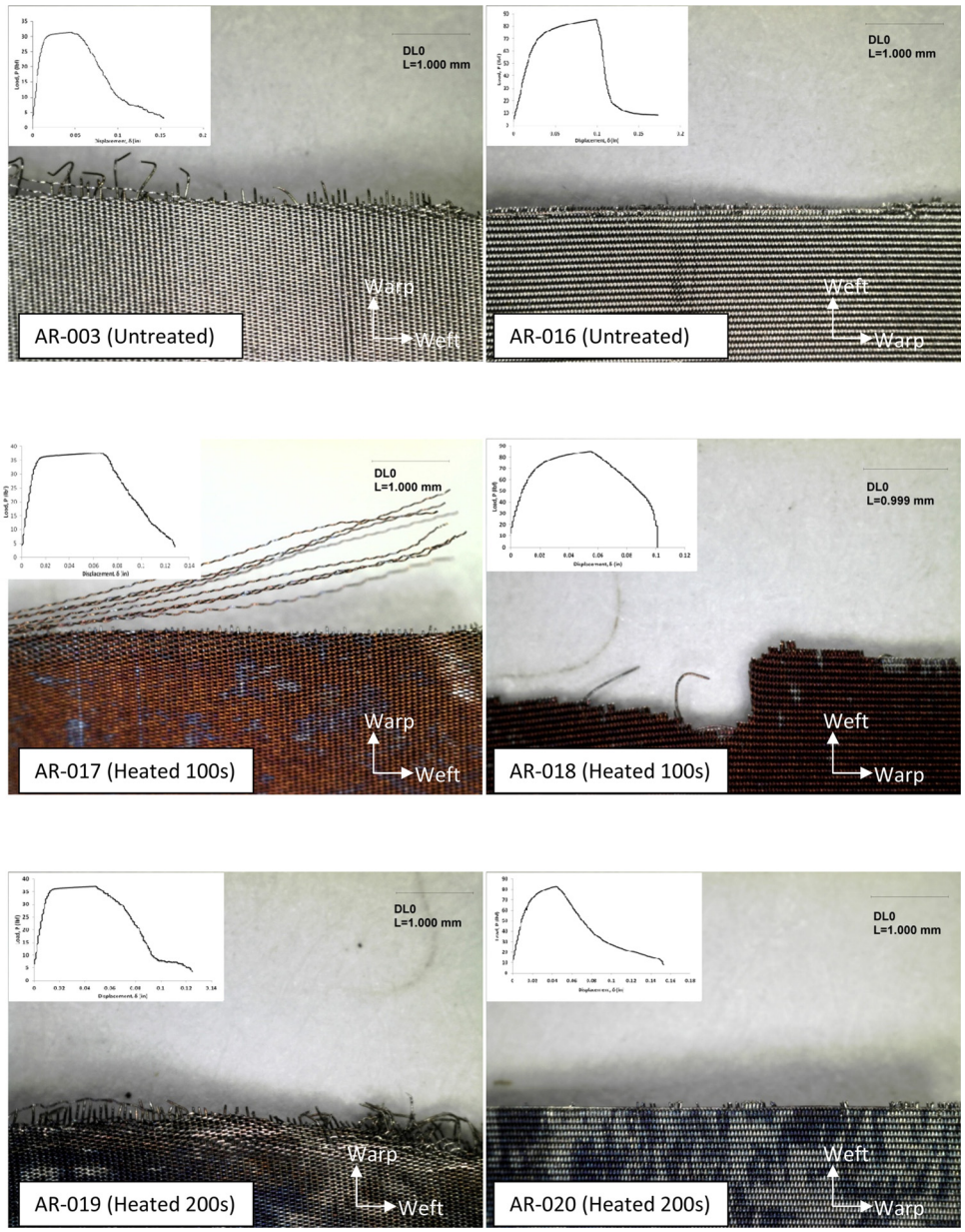

Fig. 5 Macroscale fracture surfaces of as received and heat treated 325×2300 SS316L twill dutch woven wire mesh

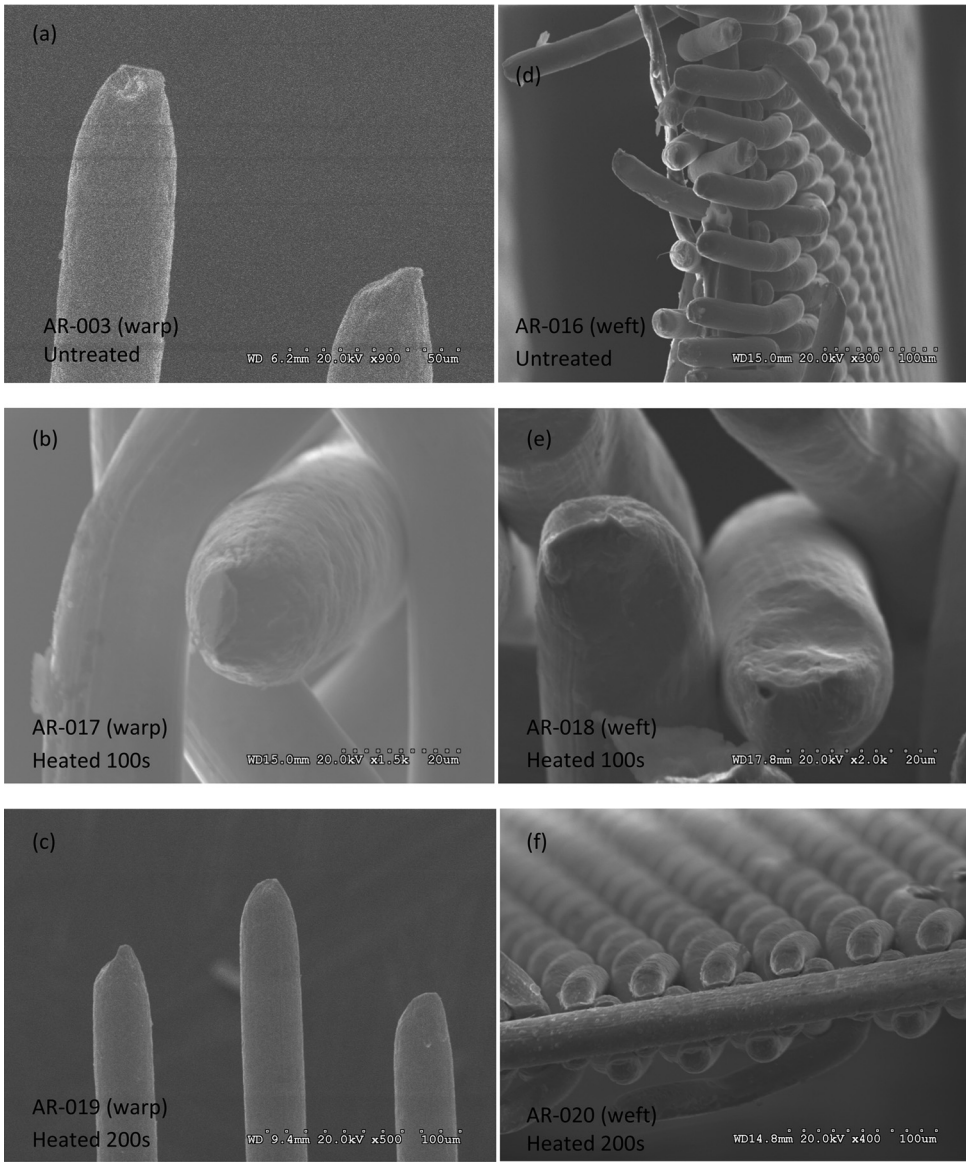

Fig. 6 Mesoscale fracture surface images (SEM) of heat treated 325 × 2300 SS316L twill dutch woven wire mesh with respect to untreated fracture surfaces

markedly increases yield strength of the as woven material in both the warp (0 deg) and weft (90 deg) directions, with increases of 23.0% and 10.2% over the untreated samples, respectively. Further investigation reveals that material stiffness is increased significantly after heat treatment, with values of 2691.4 lb/in (471.3 N/m) in the warp (0 deg) and 3902.9 lb/in (683.5 N/m) in the weft (90 deg) when heated for 100 s, representing gains of 14.5% and 30.0%, respectively. This increase in mesh stiffness can be attributed to changes in contacting wire interactions, most likely due to an increase in the coefficient of friction from oxide formation on the wire surface. This observation is supported by the fact that stiffness is increased much more substantially in the weft (90 deg) orientation, where relative wire sliding and crimp interchange are known to be dominant during portions of the elastic response [5]. The most significant material characteristic change is observed in the elongation to failure for the weft (90 deg) samples, with failure occurring at roughly half the displacement of the nonheat-treated samples. The observed reduction in ductility may be a result of the temperature at which this heat treatment was conducted. It is known that austenitic stainless steels, such as SS316L, can be affected by Chromium-Carbide precipitation at temperatures between 425 °C and 900 °C [14]. This carbide precipitation can cause sensitization and embrittlement of the steel wires, reducing toughness and ductility. It is not clear; however, the extent to which carbide precipitation embrittles the SS316L wires at such short dwell times.

3.5 Fractography. To further investigate changes in ductility and ultimate specimen failure upon heat treatment of the 325 × 2300 SS316L woven wire mesh, fractographic analysis was performed using both macroscale photography, and scanning electron microscopy of the wires post fracture. Initial investigation of the macroscale fracture surfaces reveal a few noticeable differences between the heated and nonheated specimens, particularly in the weft (90 deg) orientation, as shown in Fig. 5.

The warp (0 deg) orientation shows little discernible differences in macroscale failure surfaces after heat treatment for 100 and 200 s. An increase in weft wire pull-out is observed, but overall the fracture zone is consistent in all treated and untreated specimens. The material also exhibits clear temperature dependent color variations due to oxide formation. The observed increase in weft wire fray could be attributable to an increase in surface roughness due to the formation of oxides, which supports the

Table 6 Material properties of warp and weft wires as defined in FEM constitutive model

Property		Elastic modulus, E	Yield strength, σ_y	Ultimate tensile strength, UTS	Density, ρ	Poisson's ratio, ν
Warp	SI	200.0 GPa	464.0 MPa	599.8 MPa	0.008 g/mm^3	0.3
	English	29.0 Msi	67.3 ksi	87.0 ksi	0.289 lbf/in^3	0.3
Weft	SI	200.0 GPa	1241.0 MPa	1344.4 MPa	0.008 g/mm^3	0.3
	English	29.0 Msi	180.0 ksi	195.0 ksi	0.289 lbf/in^3	0.3

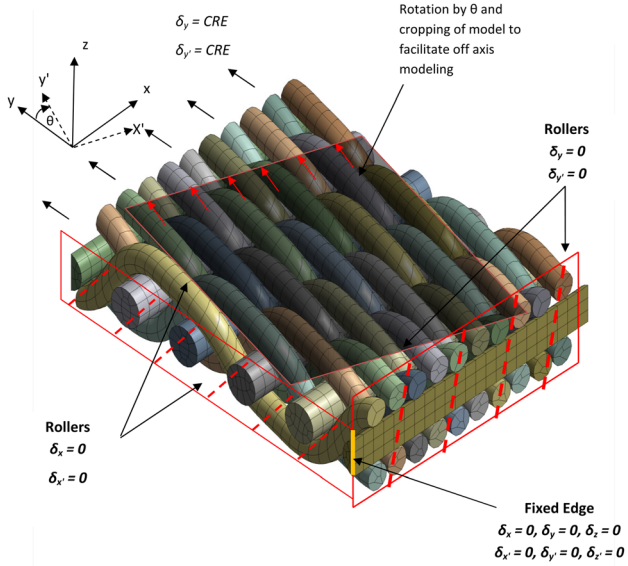

Fig. 7 Finite element mesh of 3D CAD model used to facilitate the numerical modeling of the 316 L SS woven wire mesh with boundary conditions used to simulate the tensile testing of the weft (90 deg) orientation sketched, along with illustration of rotation and cropping used to form off-axis simulation conditions

claim that changes in mesh stiffness are a product of increased contact friction.

The effects of heat treatment are more visible in the fracture zones of the weft (90 deg) oriented specimens. The as received weft (90 deg) specimen (AR-016) fractures in a straight and narrow zone, with little wire fray observed. Fracture occurs along a line of high stress due to contact with the orthogonal warp wires. Conversely, the fracture zone of the weft (90 deg) specimen heated for 100 s (AR-018) appears jagged and rough. The distributed fracture zone of AR-018 may communicate that contact stresses contribute less to the overall failure of the mesh. The observed increase in wire pullout in this specimen is attributable to the jagged fracture surface. The weft (90 deg) specimen heated for 200 s (AR-020) does not display the jagged fracture surface observed after 100 s. Aside from a change in specimen color from heating, no discernible differences are observed between the 200 s heated specimen and the as received specimen. Fracture is sharp but uniform, seeming to occur along the line of contact with a perpendicular warp wire.

The inconsistency in heat treatment effect on fracture observed in the main weave orientations suggests competing phenomenon during the heat treatment process. While strength is significantly increased without ductility loss in the warp (0 deg) orientation, significant losses of ductility accompany only moderate strength gains in the weft (90 deg) orientation. Differences in wire size, exposure, and loading mode between the two orthogonal weave directions are the most likely reasons for this difference. The weft wires are nearly 33% smaller in diameter than the warp wires, resulting in faster heating and cooling times, and ultimately different impacts on wire microstructure. Also, the warp wires are completely covered by the weft wires due to the tight mesh weaving,

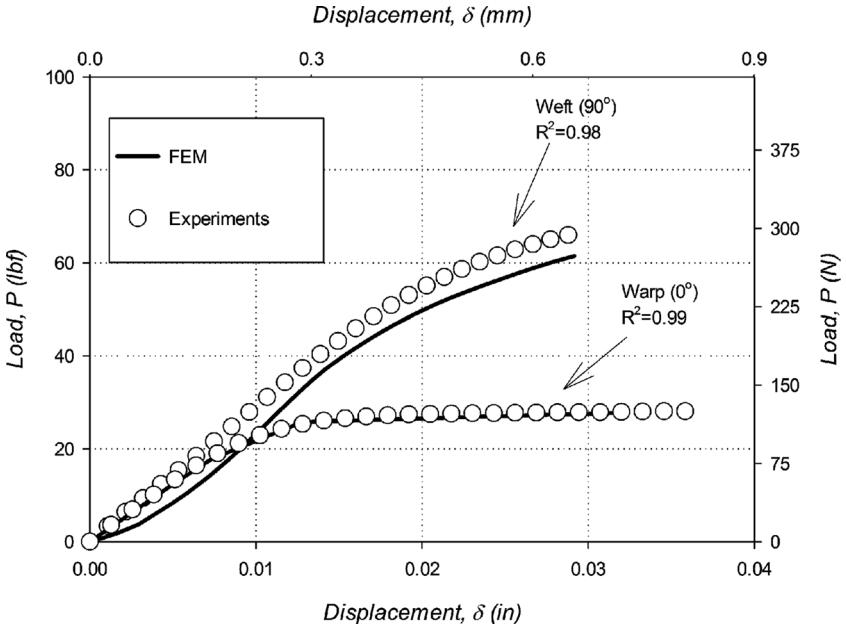

Fig. 8 The elastoplastic response of the finite element model as compared to the mechanical response of the 325 × 2300 316 L stainless steel woven wire mesh subject to tensile testing in the warp (0 deg) and weft (90 deg) orientations

resulting in less oxidation, and less severe temperature gradients than experienced by the fully exposed weft wires. These observations are supported by the material response as shown in Fig. 4, where heating reduces ductility on the smaller exposed weft wires (Fig. 4(*b*)), but markedly increases strength with no negative impact on ductility in the warp wires (Fig. 4(*a*)).

Based on the observations from macroscale fractography, a closer investigation of the fracture surfaces is warranted via scanning electron microscopy (SEM). Fractured wires of both the heated specimens and the as received specimens were compared, with specific attention paid to any changes in fracture ductility. A Hitachi model No. S3500N microscope was used to collect the images of the mesoscale fracture shown in Fig. 6.

The SEM images shown in Fig. 6 reveal that heat treatment indeed impacts ductility in the weft wires as suggested by the experimental results. Comparison of Fig. 6(*a*) (AR-003) to Fig. 6(*c*)

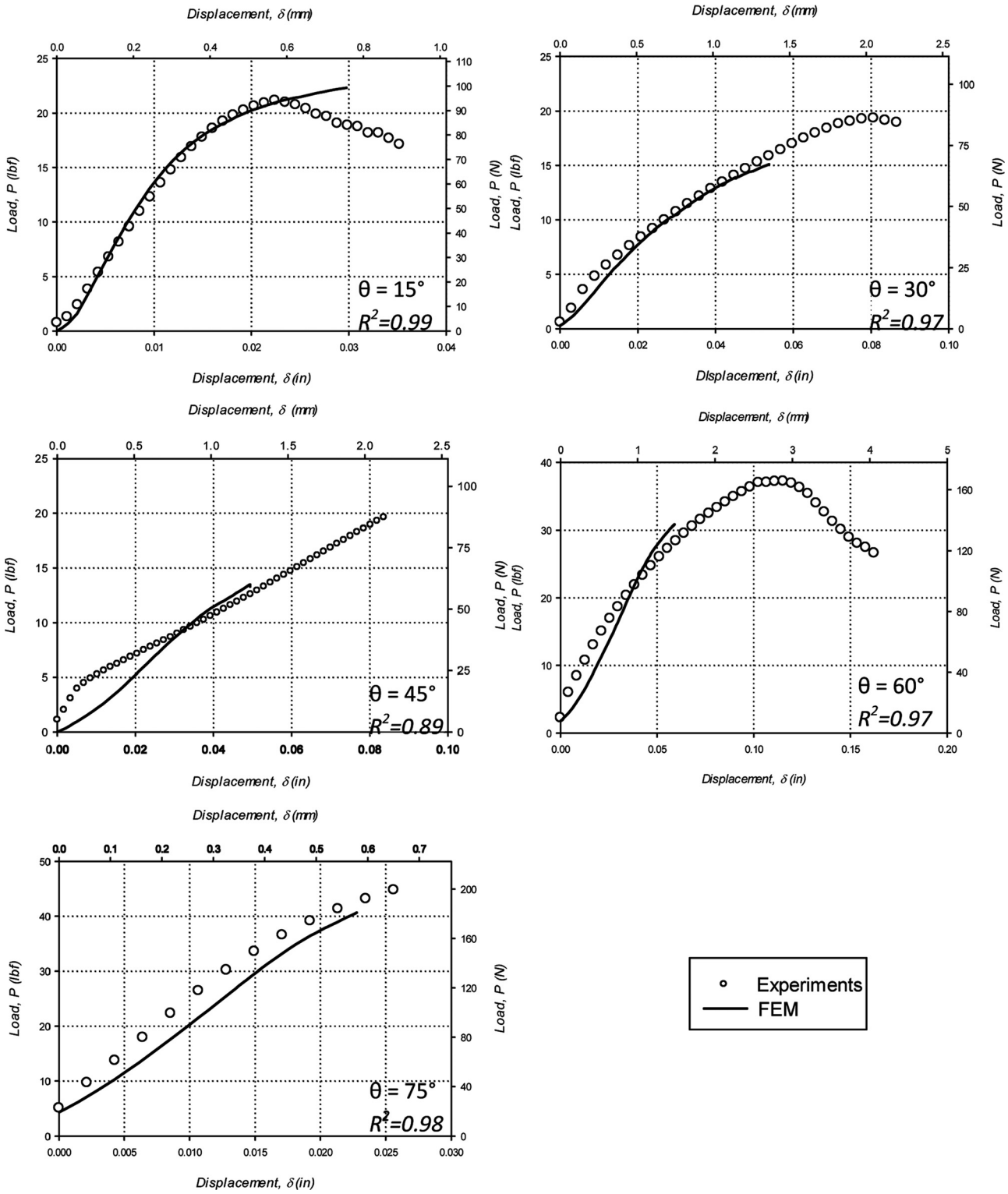

Fig. 9 Macroscale load—displacement curves from off-axis numerical simulation of 325 × 2300 SS316L woven wire mesh compared with experimental results

(AR-019) shows that no significant loss in ductility occurs in the warp wires upon heat treatment. Figure 6(*c*) displays typical ductile failure characteristics, with failure tending to occur along the 45 deg shear plane after significant plastic deformation. A comparison of the wire fracture surface area reduction of the 200 s heat treated warp (0 deg) oriented specimen (AR-019) and the as received (AR-003) warp (0 deg) orientation specimen reveals no significant difference in the amount of wire necking prior to fracture, with average reduction percentage values of 57.4% and 51.1%, respectively. In this comparison, the reduction area of the warp wires is calculated via a ratio of projected diameters measured from the SEM images, i.e.,

$$R_a = \left[1 - \left(\frac{D_f}{D_w}\right)\right] \times 100 \tag{2}$$

where R_a is the percentage of area reduction of the fracture zone, D_f is the fracture zone projected diameter, and D_w is the projected wire diameter away from the fracture zone. In general, when loaded in the warp (0 deg) direction, failure in the warp wires is typical of a pure tension loaded ductile specimen, with clearly visible areas of cup-cone type fracture along 45 deg shear planes. These characteristics, along with significant wire neck-down prior to fracture, are present in both heat treated and as received warp wires, indicating a lack of dependence of warp wire ductility on the short dwell-time. This observation, along with significant strength gains observed in this orientation, indicate that strengthening is to be expected in the warp (0 deg) orientation of the 325×2300 SS316L woven wire mesh, even in the case of the short dwell times associated with ETD applications.

As opposed to the warp wires, SEM images of weft wire fracture zones reveal distinct differences between the heat treated and as received specimens. Figure 6(*d*) (AR-016) shows a relatively broad process zone in the untreated weft (90 deg) specimen, revealing large deformations and varying fracture locations. Warp wire plastic displacement is also observed in Fig. 6(*d*), indicating that a significant amount of strain energy is accepted by the orthogonal warp wires upon loading in the weft (90 deg) direction. Load sharing between orthogonally woven wires likely leads to the high elongation to failure observed in untreated weft (90 deg) specimens. Heat treatment produces much more concentrated fracture zones in weft (90 deg) oriented specimens as illustrated by Fig. 6(*f*). Also, warp wire plasticity has been significantly reduced in the 200 s heat treated weft (90 deg) oriented specimen (AR-020), indicating a reduction in crimp interchange caused by ductility loss in the weft wires. The combination of fracture zone concentration and a clear reduction in orthogonal wire interaction observed in heat treated weft (90 deg) specimens is consistent with experimental results, indicating moderate increases in strength and stiffness coupled with embrittlement. It is noted that wire scale strain measurements would serve to clarify the mechanisms leading to fracture in this material, and this research is left to future work.

4 Numerical Simulation

4.1 Model Definition. Numerical simulations were conducted to model the behavior of SS316L woven wire mesh subject to various stress states. To carry out these simulations, a 3D mesoscale finite element model was created using ANSYS. This simulation technique requires that individual wires be modeled, both geometrically and constitutively, and employs 3D contact elements to define frictional wire contact and allow relative wire sliding. The model was designed to facilitate comparability to the tensile experiments, with controlled displacements being applied uniaxially to the mesh. Material properties were defined for each wire type (warp or weft) independently, with the goal being to match the material response of the tensile specimens from the warp (0 deg) and weft (90 deg) orientations. This entails a parametric process in which each property is iteratively selected to achieve optimal curve-fit to the experimental data. Defined elastic constants, such as the Elastic Modulus and Poisson's ratio, were forced to conform with the published properties for SS316L, while properties such as strength, friction coefficient, contact stiffness, and hardening parameters were optimized to achieve optimal correlation with experimental results. It must be noted that phenomenological influences such as residual plasticity in the wires, or geometrical disparities in the mesh, are not explicitly captured in this modeling effort, but instead are taken into account by iterative maximization of the regression coefficient between the numerical model and experimental load-deflection relationships. As predicted by Eq. (1), the wire strengths defined in the model vary somewhat from published properties for SS316L, as shown in Table 6; however, overall the response of the model is exceptional given the geometric complexity. To investigate the elasto-plastic response of the mesostructure, a multilinear kinematic hardening (MKIN) model was employed for the warp and weft wires based on published tensile curves for SS316L [13].

The boundary conditions chosen for this modeling effort reflect the need for easy comparison to experimental data. Displacement was applied to one face of the model via a scaled rate identical to the tensile experiments. Symmetry constraints were then applied to the free edges of the mesh geometry via frictionless supports, as illustrated in Fig. 7.

To capture the behavior of the SS316L twill dutch woven wire mesh in the first quadrant of σ_1-σ_2 space, a series of uniaxial tensile experiments were conducted in various material orientations, ranging from 0 deg (warp) to 90 deg (weft) in 15 deg intervals. Capturing this behavior via the mesoscale finite element model can be realized through one of two methods. One option is to rotate the stress state imparted onto the model to match that of each experimental orientation. This method helps ensure proper stress distribution, and lends itself conveniently towards parametric modeling. The use of this method via controlled displacement boundary conditions, however, requires the definition of complex boundaries to ensure the applied displacement is dependent on the strain of previous load step. To eliminate this difficulty, it was elected to rotate and crop the model geometry to each respective orientation, and then to apply a uniaxial controlled displacement to the rotated specimen. This boundary condition, also illustrated in Fig. 7, assures easy comparison to the experimental data, and

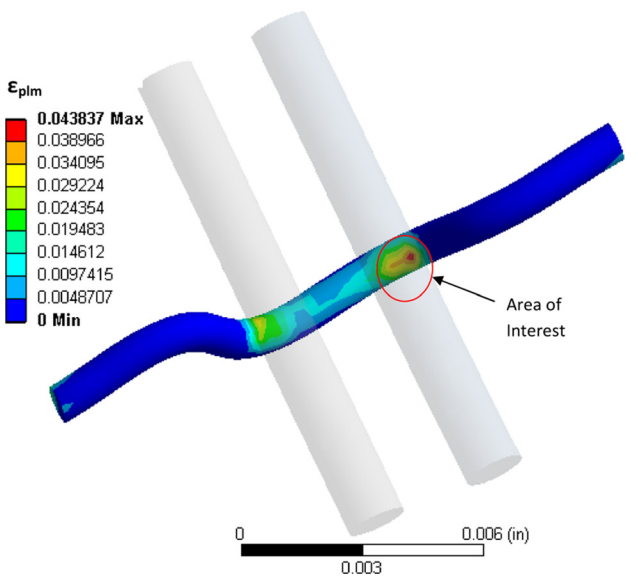

Fig. 10 Example area of interest for investigation of mesoscale plastic strain development in the 325 × 2300 SS316L twill dutch woven wire mesh

achieves shearing strains on the material through shear coupling effects as in the uniaxial experiments.

4.2 Model Results. The model was exercised in a parametric fashion to test the mesoscale response of the woven wire mesh in every material orientation tested experimentally. The warp (0 deg) and weft (90 deg) orientations serve as benchmarks for the identification of the wire material properties, and so serve as good indicators of how well the model behaves with respect to experimental data. The simulated load versus displacement response of the main weave axes is provided in Fig. 8 in conjunction with the experimental results. The fit is exceptional through the elasto-plastic region in both axes, validating the ability of the simplistic

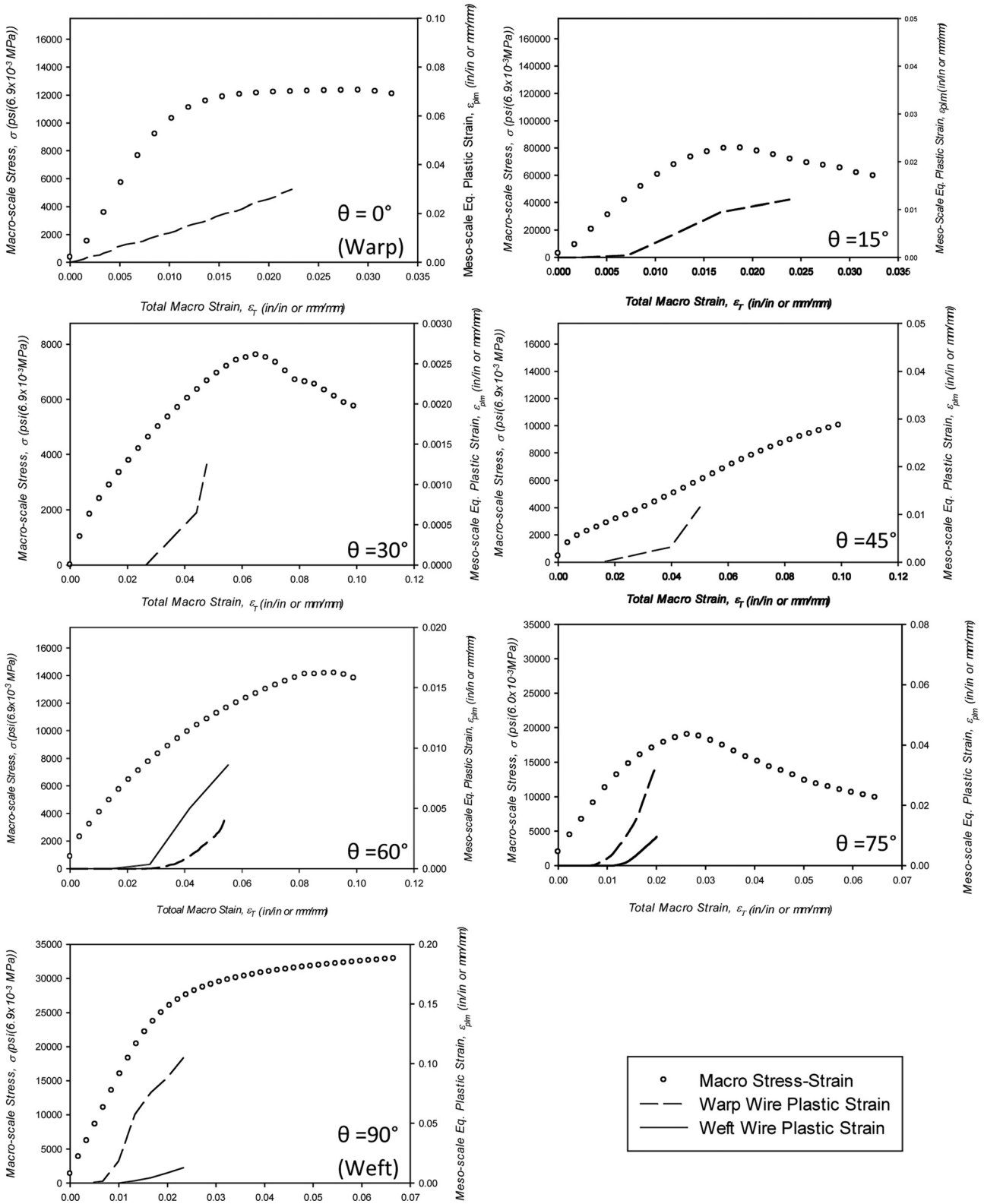

Fig. 11 The development of plastic strain at the mesoscale predicted by the numerical simulations with respect to the global stress-strain relationship of the 325 × 2300 SS316L woven wire mesh at various material orientations

constitutive model to capture the macroscopic response of the material.

Off-axis simulations were necessary to show that the mesoscale response of the SS 316 L woven wire mesh could be related to the macroscale response for all tension loading modes. Good agreement between mesoscale numerical results and macroscale test results in all material orientations is necessary to justify the use of global constitutive assumptions to model this material. Such results in all orientations allow the design engineer to homogenize the mesostructure of the mesh, and develop strength and life predictions based solely on easily obtainable macroscale material characteristics. The load versus displacement response of the numerical simulations in each off-axis orientation is provided in Fig. 9, along with their respective experimental curve. Inspection of Fig. 9 shows that the mesoscale model response closely follows the response of the macroscale in the elastoplastic region. This fact justifies the use of homogenized orthotropic material properties to model this material, alleviating the need to consider the geometry or characteristics of the ensemble of wires in the mesh. The exceptional fit of the mesoscale model response to experimental data in most orientations also justifies the development of a 2D orthotropic finite element to model higher-level mechanical aspects of this material, such as fatigue and damage characteristics.

4.3 Mesoscale Yield Behavior. The global mechanical behavior of a composite material is in general a function of its constituents. Typically, the material properties of the individual components and the interactions between the different substrates govern the global response of the material. Woven materials like the SS316L twill dutch woven wire mesh in question are similarly dependent on the behavior and interaction of their components. The mesoscale characteristics of the mesh, such as the weave pattern, tightness, and uniformity, ultimately determine its global behavior. Evolution of the global behavior of the mesh throughout elastoplastic transition is a function of the behavior of the individual wires in the weave. The material properties, geometry, and contact parameters of the wires are important factors in the overall mesh behavior, and a thorough understanding of mesh yielding requires investigation of these influences.

Woven materials possess an intermediate level of internal component interaction not encountered in homogenous materials. An intermediate scale of material evolution, in which individual wires begin to yield at the mesoscale, exists between the microstructural accumulation of defects and the global evolution of the material. In the same manner that accumulation of damage at the microscale ultimately leads to global yielding in homogenous materials, accumulation of plasticity at the mesoscale leads to global yielding of the woven wire mesh. It is postulated that wire level yielding reaches some critical value prior to any discernable deviation of the macroscale material response from elastic behavior. In this light, mesoscale plasticity accumulation prior to global mesh yielding can be viewed as macroscale elastic damage accumulation.

To investigate the relationship between localized wire yielding and global yielding of the 325×2300 SS316L twill dutch woven wire mesh, further numerical simulations were conducted with the goal of mapping the progression of wire level plastic deformation with respect to the macroscale response. The developed finite element model, constrained in an identical fashion as described in Fig. 7, was used along with the MKIN model to simulate the development of local plastic strain at the mesoscale of the mesh. Plastic strain was recorded at key areas on the individual wires, typically at points of contact where plasticity was the highest, as illustrated in Fig. 10. These areas were carefully chosen from central locations in the mesh such that boundary effects were minimal, but it must be noted that the reported plastic strains are local, and not indicative of overall wire plasticity. The progression of local plastic strain in the wire level is related to the global response of the woven mesh by plotting the global macrolevel experimental stress-strain relationship with respect to mesoscale plastic strain accumulation. This relationship is illustrated in Fig. 11 for various material orientations.

Analysis of Fig. 11 reveals a definite dependence of wire plasticity evolution on material orientation, and provides some evidence to suggest that localized plastic deformation indeed reaches some critical value at the mesoscale prior to global yielding of the woven mesh. It is observed, particularly in the weft dominant orientations (60 deg–90 deg), that significant wire level plasticity develops prior to the material exhibiting signs of global yielding. This behavior indicates that individual wire yielding is indeed a source of elastic damage that may affect the global elasticity of the woven mesh. Damage, in this case, typically defined as the accumulation of microstructural defects within a material, could be defined by plasticity developing at the intermediate mesoscale. Future work is planned to develop a relationship for the development of wire level plasticity to macroscale elastic damage through continuum damage mechanics.

5 Conclusions

The elastoplastic behavior of a twill dutch woven wire mesh has been investigated via tensile experiments and FEM. It has been shown through tensile experiments and fractographic analysis that strengthening via short dwell-time heat treatment similar to ETD exposure parameters is possible on this class of materials, but with the proviso that reductions in ductility could result. Employment of the mesoscale FEM at various material orientations has revealed exceptional fit to global experimental data, justifying the use of simplified orthotropic models to develop strength or damage predictions by design engineers. Wire interactions have been studied using FEM, and it has been observed that accumulation of local wire level plastic deformation ultimately leads to global mesh yielding, and can therefore be classified as mesoscale elastic damage.

References

[1] Kawabata, S., Niwa, M., and Kawai, H., 1964, "The Finite Deformation Theories of Plain Weave Fabric, Part 1—The Biaxial-Deformation Theory," J. Text. Inst., **64**, pp. 21–46.

[2] Kumazawa, H., Susuki, I., Morita, T., and Kuwabara, T., 2005, "Mechanical Properties of Coated Plain Weave Fabrics Under Biaxial Loads," Trans. Jpn. Soc. Aeronaut. Space Sci., **48**(160), pp. 117–123.

[3] Zheng, J., Takatera, M., Inui, S., and Shimizu, Y., 2008, "Measuring Technology of the Anisotropic Tensile Properties of Woven Fabrics," Text. Res. J., **78**(12), pp. 1116–1123.

[4] Chen, S., Ding, X., and Yi, H., 2007, "On the Anisotropic Tensile Behaviors of Flexible Polyvinyl Chloride-Coated Fabrics," Text. Res. J., **77**(6), pp. 369–374.

[5] Cavallaro, P., Sadegh, A., and Quigley, C., 2007, "Decrimping Behavior of Uncoated Plain-Woven Fabrics Subjected to Combined Biaxial Tension and Shear Stresses," Text. Res. J., **77**(6), pp. 404–416.

[6] Tarfaoui, M., and Drean, J. Y., 2001, "Predicting the Stress-Strain Behavior of Woven Fabrics Using the Finite Element Method," Text. Res. J., **71**(9), pp. 790–795.

[7] Nicolleto, G., and Riva, E., 2004, "Failure Mechanisms in Twill-Weave Laminates: FEM Predictions vs. Experiments," Composites, Part A, **35**, pp. 787–795.

[8] Barbero, E. J., Trovillion, J., Mayugo, J. A., and Sikkil, K. K., 2006, "Finite Element Modeling of Plain Weave Fabrics From Photomicrograph Measurements," Compos. Sturct., **73**, pp. 41–52.

[9] Kraft, S., and Gordon, A. P., 2011, "Characterization of the Mechanical Behavior of a Metallic Fiber Woven Structure," Text. Res. J., **81**(12), pp. 1249–1272.

[10] Gibson, R. F., 2007, *Principles of Composite Material Mechanics*, CRC Press, Boca Raton, FL.

[11] Smits, A., Van Hemelrijck, D. V., Philippidis, T. P., and Cardon, A., 2006, "Design of a Cruciform Specimen for Biaxial Testing of Fiber Reinforced Composite Structures," Compos. Sci. Technol., **66**, pp. 964–975.

[12] Makinde, A., Thibodeau, L., and Neale, K. W., 1992, "Development of an Apparatus for Biaxial Testing Using Cruciform Specimens," Exp. Mech., **32**(2), pp. 138–144.

[13] Antoun, B. R., and Song, B., 2009, "Interaction of Hydrogen and Deformation in 316L Stainless Steel," Proceedings of the SEM Annual Conference, Albuquerque, NM, June 1–4.

[14] ASM International, 1998, *ASM Metals Handbook, 2nd Desk Edition*, ASM International, Materials Park, OH.